A structural health monitoring system based on multifractal detrended cross-correlation analysis

Tzu-Kang Lin[*] and Yi-Hsiu Chien[a]

Department of Civil Engineering, National Chiao Tung University, 1001 University Road, Hsinchu 300, Taiwan

Abstract. In recent years, multifractal-based analysis methods have been widely applied in engineering. Among these methods, multifractal detrended cross-correlation analysis (MFDXA), a branch of fractal analysis, has been successfully applied in the fields of finance and biomedicine. For its great potential in reflecting the subtle characteristic among signals, a structural health monitoring (SHM) system based on MFDXA is proposed. In this system, damage assessment is conducted by exploiting the concept of multifractal theory to quantify the complexity of the vibration signal measured from a structure. According to the proposed algorithm, the damage condition is first distinguished by multifractal detrended fluctuation analysis. Subsequently, the relationship between the q-order, q-order detrended covariance, and length of segment is further explored. The dissimilarity between damaged and undamaged cases is visualized on contour diagrams, and the damage location can thus be detected using signals measured from different floors. Moreover, a damage index is proposed to efficiently enhance the SHM process. A seven-story benchmark structure, located at the National Center for Research on Earthquake Engineering (NCREE) , was employed for an experimental verification to demonstrate the performance of the proposed SHM algorithm. According to the results, the damage condition and orientation could be correctly identified using the MFDXA algorithm and the proposed damage index. Since only the ambient vibration signal is required along with a set of initial reference measurements, the proposed SHM system can provide a lower cost, efficient, and reliable monitoring process.

Keywords: multifractal; detrended fluctuation analysis; detrended cross-correlation analysis; structural health monitoring

1. Introduction

Over the past two decades, implementing strategies for preventing considerable loss of human life and property has become a global issue. Structural health monitoring (SHM) is aimed at diagnosing damage conditions and pinpointing damage locations. Depending on the method for determining the level of structural damage, SHM methods can be divided into two main categories: global health monitoring and local health monitoring.

Global health monitoring methods are used to detect information about an entire structure, and such approaches reveal the characteristics of damage according to the changes in the global dynamic properties of a structure, such as the damping ratio, mode shape, and frequency. In last decades, the monitoring techniques were well developed base on the vibration test (Yun 2012, Li *et al*. 2015). Several examples of well-known global health monitoring techniques are the mode shape curvature-based method (Pandey *et al*. 1991), mode shape-based method (Farrar and James 1997), and natural frequency-based method (Fan and Qiao 2011).

Local health monitoring methods are applied to observe the behavior of potential damage locations or critical areas and to track the scale of damage. Several techniques have been developed for damage location diagnosis, and such techniques are based on a few simple concepts such as visual inspection (Aktan and Catbas 2003), strain and displacement (Jang *et al*. 2007), and inclinometers (Pehlivana and Bayata 2016). Although global health monitoring techniques can assess the existence of damage, locating the damage and quantifying the damage severity level are relatively difficult. Moreover, time-consuming processes, high cost, and high accuracy requirements are all problems that render local health monitoring techniques more difficult to apply than global health monitoring techniques. In current research trends, the combination of both methods is essential for SHM.

Mandelbrot (1983) studied the shape of nature and discovered the fractal phenomena. The contours of rocks or other natural phenomena show similarity in different scales. Fractal scaling behavior can be applied to interpret the complex, irregular, nonstationary, and fragmented changes in shape and time series (Peng *et al*. 1995, Kantelhardt 2008). Many algorithms have been developed to describe the scaling behavior based on fractal theory, and the advantages and limitations of such algorithms have been compared.

Ivanov *et al*. (1999) studied the multifractality of the human heartbeat from a biological dynamical system. They uncovered a loss of multifractality for congestive heart failure, demonstrating an explicit relationship between the

---
*Corresponding author, Associate Professor
 E-mail: tklin@nctu.edu.tw
[a]Master Student

nonlinear features of the condition. Kantelhardt *et al*. (2002) proposed the multifractal detrended fluctuation analysis (MFDFA) method, a generalization of detrended fluctuation analysis (DFA) based on fractal theory. Ihlen (2012) applied MFDFA for estimating the multifractal spectrum of biomedical time series. The multifractal spectrum reflected variations in the fractal structure of the biomedical time series and identified pathological conditions. In addition, Dutta *et al*. (2013) applied MFDFA to study the human gait time series for Parkinson's disease, Huntington's disease, and individuals uninhibited by either condition. The results revealed that long-range correlation was responsible for multifractality and that the degree of multifractality of the normal set was greater than that of the diseased set. The MFDFA method can distinguish between normal sets and diseased sets. Recently, Haris *et al*. (2014) applied MFDFA to animal vocalizations, involving seahorse feeding clicks, to compare the body, sex, size, and weight of a seahorse; this work underscored the versatility of the MFDFA method in investigating bioacoustic observations and nonlinearities. In many studies, the multifractal properties of natural phenomena are validated by MFDFA; however, this method is not sufficient for determining the details of different sets. In the field of civil engineering, Su *et al*. (2016) utilized MFDFA to identify the fractal characteristics in the measured time series of dam structural behavior. Then, the iterated function system algorithm is studied to build the fitting model. Finally, the iterated function system is combined with the variable dimension fractal model to build the forecasting modal of dam structural behavior.

Zhou (2008) proposed a method called multifractal detrended cross-correlation analysis (MFDXA), which is based on detrended covariance, for investigating the multifractal behaviors between two time series or high-dimensional quantities. The MFDXA method was applied to the daily closing prices of the Dow Jones Industrial Average and National Association of Securities Dealers Automated Quotation indices, showing a power-law dependence with positive q-order. In earthquake engineering, Shadkhoo (2009) used MFDXA to investigate the cross-correlation of temporal and spatial interevent seismic data; the results showed that the interevents of temporal and spatial seismic series exhibited weak multifractality, despite their strong multifractal behavior. In the financial field, a previous study applied MFDXA to investigate the cross-correlation of agricultural futures markets in two highly correlated economies: China and the United States (He 2011). The study validated the strong cross-correlation of the agricultural futures markets of China and the United States, which share similar multifractal structures. Moreover, Wang (2013) found that price and load time series in the California power market and JPM power market exhibited a long-term correlation. In the biomedical field, Ghosh *et al*. (2014) used MFDXA to study the electroencephalographic data of epileptic patients in 2014; they revealed the degree of cross-correlation to be higher among seizure and seizure-free intervals in the epileptogenic zone, indicating that the data are significant for diagnosis. Recently, Dutta *et al*. (2016) studied the human gait pattern of disease-free individuals and patients suffering from Parkinson's disease.
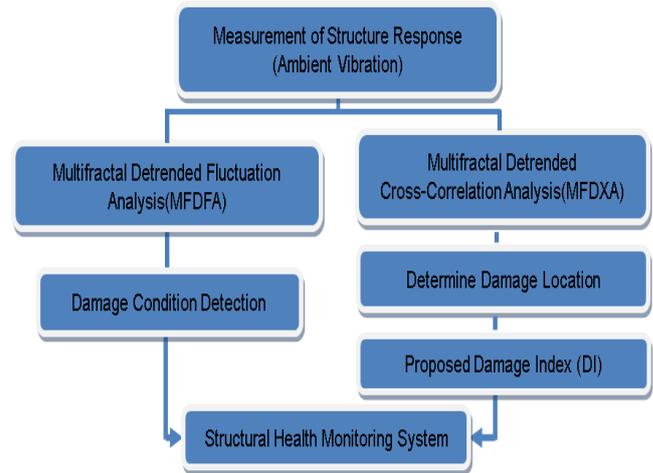

Fig. 1 Flowchart of the proposed SHM system

They revealed that the degree of multifractality and the degree of correlation were greater for the disease-free set than for the diseased set, verifying that the results of the MFDFA method were not sufficient for distinguishing between the two sets. Nie *et al*. (2016) investigated the long-range cross-correlation between urban impervious surface and land surface temperatures with detrended cross-correlation analysis and multifractal detrended cross-correlation analysis. The observed correlations show the cahange of the urbanization of Shanghai in early 21st century. In summary, the above-mentioned literatures show the potential ability to analyze complex signal in numerous fields.

Over the past decades, MFDFA and MFDXA have provided outstanding findings in various fields, especially biomedicine, economics, and finance. As reliabilty and practicability are still the core concern hindering the existing SHM methods, the main goal of this study was to provide a novel insight in the field of SHM by exploiting the advantages of MFDFA and MFDXA for damage condition and location detection. MFDFA was introduced to determine the damage condition of a structure by measuring the dynamic signal from a single sensor on each floor. Moreover, MFDXA was used for locating the damaged floor of the structure. The flowchart of the proposed SHM system is shown in Fig. 1, and the remainder of this paper is organized as follows: First, the basic concepts of MFDFA and MFDXA, and the proposed damage index are described. Second, based on a practical experimental verification process conducted using a seven-storey steel benchmark structure located at the National Center for Research on Earthquake Engineering (NCREE), the damage condition and location are assessed. Finally, a summary is presented and conclusions are drawn.

2. Proposed SHM method

2.1 Multifractal detrended fluctuation analysis

A brief theoretical overview is presented in this section. For a time series of finite length N, the first step involves

the subtraction of the mean X_{ave} from the vibration time series $X(i)$.

$$X_{ave} = \frac{1}{N}\sum_{i=1}^{N} X(i) \tag{1}$$

$$Y(i) \equiv \sum_{k=1}^{i}[X(k) - X_{ave}] \quad \text{for } i = 1...N. \tag{2}$$

$Y(i)$ is defined as the cumulated data series, which is divided into N_s nonoverlapping bins of equal length s, $N_s=int(N/s)$. To avoid omitting the short segment at the end of the profile, the same process is repeated from the opposite end of the time series. Hence, $2N_s$ bins are obtained, and the local linear trend for each bin is calculated by a least-square fitting for each segment v. For $v=1,2,...,N_s$, the variance is calculated by

$$F^2(s,v) = \frac{1}{s}\sum_{i=1}^{s}\{Y[(v-1)s+i] - y_v(i)\}^2 \tag{3}$$

for each segment v, $v=N_s+1,...2N_s$

$$F^2(s,v) = \frac{1}{s}\sum_{i=1}^{s}\{Y[N-(v-N_s)s+i] - y_v(i)\}^2 \tag{4}$$

where $y_v(i)$ is the linear fitting polynomial in the segment v. Finally, for each of the $2N_s$ segments, the q-order fluctuation function is obtained.

$$F_q(s) = \left\{\frac{1}{2N_s}\sum_{v=1}^{2Ns}\left[F^2(s,v)\right]^{\frac{q}{2}}\right\}^{\frac{1}{q}} \tag{5}$$

In general, q can be any real value except zero. For $q = 0$,

$$F_0(s) \equiv \exp\left\{\frac{1}{4N_s}\sum_{v=1}^{2Ns}\ln\left[F^2(s,v)\right]\right\} \tag{6}$$

The scaling behavior of the fluctuation function is determined by analyzing the slope of the log-log plots, $F_q(s)$ versus s for different q. If the series $X(i)$ exhibits a long-range power-law correlation, $F_q(s)$ with s is described as

$$F_q(s) \propto s^{H(q)} \tag{7}$$

where $H(q)$ is the slope and can be considered the generalized q-order Hurst exponent. For a stationary time series, where q is equal to 2, $H(2)$ is identical with the Hurst exponent. The positive and negative values of q describe scaling behaviors with large and small fluctuations, respectively.

$H(q)$ is directly related to the classical scaling exponent $\tau(q)$. The relationship between $H(q)$ and $\tau(q)$ can be represented as

$$\tau(q) = q \times H(q) - 1 \tag{8}$$

Another means of characterizing a multifractal series is with the singularity spectrum, also termed the q-order singularity dimension Dq, which is related to $\tau(q)$ through a Legendre transform:

$$hq = \tau'(q) = H(q) + q \times H'(q) \tag{9}$$

$$Dq = q \times hq - \tau(q) \tag{10}$$

where hq is the singularity exponent or strength, and Dq represents the dimension of the subset of the series.

For an N-floor structural dynamic time series, the existing multifractal properties can be verified by MFDFA; however, as MFDFA does not consider the influence of signals between different floors, the damage location cannot be reflected by applying the MFDFA process.

2.2 Multifractal detrended cross-correlation analysis

MFDXA is adopted to study the degree of correlation between two nonstationary time series. Considering two time series $X(i)$ and $Y(i)$ of length N, where $i=1, 2.., N$, the accumulated deviation series are formed by subtracting the mean values of X_{ave} and Y_{ave} from their time series, respectively.

$$Y(i) \equiv \sum_{k=1}^{i}\left[X(k) - X_{ave}\right] \tag{11}$$

$$Y_2(i) \equiv \sum_{k=1}^{i}\left[X_2(k) - X_{2_{ave}}\right] \tag{12}$$

The integration can reduce the level of measurement noise presented in the experimental data. Each of the accumulated series are divided into N_s nonoverlapping bins of equal length s, $N_s=int(N/s)$. According to this step of the MFDFA procedure, $2N_s$ segments are obtained. Concurrently, for $v=1,2,...,N_s$, the covariance is calculated by

$$F(s,v) = \frac{1}{s}\sum_{i=1}^{s}\{Y[(v-1)s+i] - y_v(i)\} \times \{Y_2[(v-1)s+i] - y_{2_v}(i)\} \tag{13}$$

and for each segment v, $v=N_s+1,...2N_s$

$$F(s,v) = \frac{1}{s}\sum_{i=1}^{s}\{Y[N-(v-N_s)s+i] - y_v(i)\} \times \{Y_2[N-(v-N_s)s+i] - y_{2_v}(i)\} \tag{14}$$

where $x_v(i)$ and $y_v(i)$ are the fitting polynomials in the segment v. The q-order detrended function $F_q(s)$ is then obtained after averaging two N_s bins.

$$F_q(s) = \left\{\frac{1}{2N_s}\sum_{v=1}^{2Ns}\left[F(s,v)\right]^{q/2}\right\}^{1/q} \tag{15}$$

When q is equal to zero, F_q is infinite. A logarithmic averaging procedure is applied as follows

$$F_0(s) \equiv \exp\left\{\frac{1}{4N_s}\sum_{v=1}^{2Ns}\ln\left[F(s,v)\right]\right\} \tag{16}$$

This procedure is repeated by varying the value of s. If

the series have a long-range power-law correlation, then $F_q(s)$ exhibits power-law behavior

$$F_q(s) \propto s^{\lambda(q)} \tag{17}$$

The scaling exponent $\lambda(q)$ represents the degree of cross-correlation between the two series.

For positive q, $\lambda(q)$ describes the scaling behaviors of segments with large fluctuations, and for negative q, $\lambda(q)$ describes the scaling behaviors of segments with small fluctuations. $\lambda(q)=0.5$ indicates an absence of cross-correlation; $\lambda(q)>0.5$ indicates persistent long-range cross-correlation, where a high value in one variable is likely to be followed by a high value in another variable; and $\lambda(q)<0.5$ indicates antipersistent cross-correlation, where a high value in one variable is likely to be followed by a low value in another variable (Sadegh Movahed 2008). When the damage occurs, the covariance surfaces of damaged floors show significant differences with other surfaces.

2.3 Proposed damage index

To improve the accuracy of the SHM system in diagnosing the damage location of a structure, a damage index is proposed. The detrended covariance of a healthy case is set as the reference value, and thus, the detrended covariance for different q-orders and scales is processed to obtain the damage index.

The signal measured from the ground floor was cross-correlated with that of the other floors. For a structure with N floors, a total of N+1 MFDXA curved surfaces can be derived: $G*G$, $G*1F$, $G*2F$, ..., $G*NF$. The undamaged and damaged conditions are expressed respectively as

$$F_q^{damaged}(s) = \left\{ D_{G*G}, D_{G*1F}, D_{G*2F}, ..., D_{G*NF} \right\}^T \tag{18}$$

$$F_q^{undamaged}(s) = \left\{ U_{G*G}, U_{G*1F}, U_{G*2F}, ..., U_{G*NF} \right\}^T \tag{19}$$

The symbol D_{G*G} represents the $G*G$ surface for the damaged structure. Similarly, U_{G*G} represents the $G*G$ surface for the undamaged structure. To clarify the change between each cross-correlated surface in one damaged case, the difference between all adjacent floor pairs is calculated, and the difference over the surface is summarized to present the condition of each floor.

The damaged case and undamaged case can be expressed respectively as follows

$$FD = \left\{ \sum(D_{G*1F} - D_{G*G}), \sum(D_{G*2F} - D_{G*1F}), ..., \sum(D_{G*NF} - D_{G*(N-1)F}) \right\}^T \text{ , and} \tag{20}$$

$$FU = \left\{ \sum(U_{G*1F} - U_{G*G}), \sum(U_{G*2F} - U_{G*1F}), ..., \sum(U_{G*NF} - U_{G*(N-1)F}) \right\}^T \tag{21}$$

After *FD* and *FU* are derived, the proposed damage index for a specific floor can be expressed as

$$DI_i = \left\{ FU_i \right\} - \left\{ FD_i \right\} \tag{22}$$

Table 1 Details of experimental structure

Items	Size
Height of each floor	110 cm
Floor area	150x110 cm
Column	150x25 mm
Bracing	65x65x6 mm
Additional mass	500 kg/floor

where i represents the floor number. A positive damage index value indicates the absence of damage, which means that the covariance of a specific floor does not change significantly; whereas a negative damage index value indicates the existence of damage on the floor, because of the sharp covariance variation of the damaged floor.

Since a negative q value tends to reflect the behavior of small fluctuations easily influenced by ambient interference, this study considered q values ranging from 1 to 5 for damage index diagnosis. Moreover, for the instability of the ambient vibration signal, the covariance Fq is normalized to prevent extreme values that influence the accuracy of the damage index.

3. Description of experimental data

A seven-story benchmark structure, located at the NCREE, was employed for experimental verification to demonstrate the performance of the proposed SHM system. A total of eight velocity sensors were mounted both on the benchmark structure and at ground level.

The dimensions of the scaled-down steel specimen are presented in Fig. 2(a). The height, length, and width of each story were 1.1, 1.5, and 1.1 m, respectively. L-shaped steel angles measuring 65×65×6 mm were adopted for bracing the structure. An additional mass of 500 kg was applied to each floor to simulate the practical structural characteristics. A VSE-15D velocity sensor manufactured by Tokyo Sokushin Co., Ltd., was used for the experiment and installed in the center of each floor for data acquisition. Layouts of a single floor is shown in Fig. 2(b), and the details of the experimental specimen are listed in Table 1.

Damage was simulated by removing the two installed bracings in the weak axis direction for every story. The removal of the bracings indicated a change in the stiffness of the structure at a certain story as the cause of potential damage. Figs. 2(c) and (d) show the detailed bracing of the experiment. To roughly reflect the stiffness variation caused by the removal of the bracings, Fast Fourier Transform (FFT) was conducted to evaluate the corresponding structural frequency, and the result is showed in Table 2. The gradually decreasing trend of the frequency implies the reduction of the stiffness. However, the slight variations in the cases of damage on the low floors may be affected by the temperature and other environmental variables (Yan *et al*. 2005). The proposed SHM system is designed for operation modal analysis, where the properties of a structure is identified based on vibration data collected when the structure is under ambient vibration. To avoid any
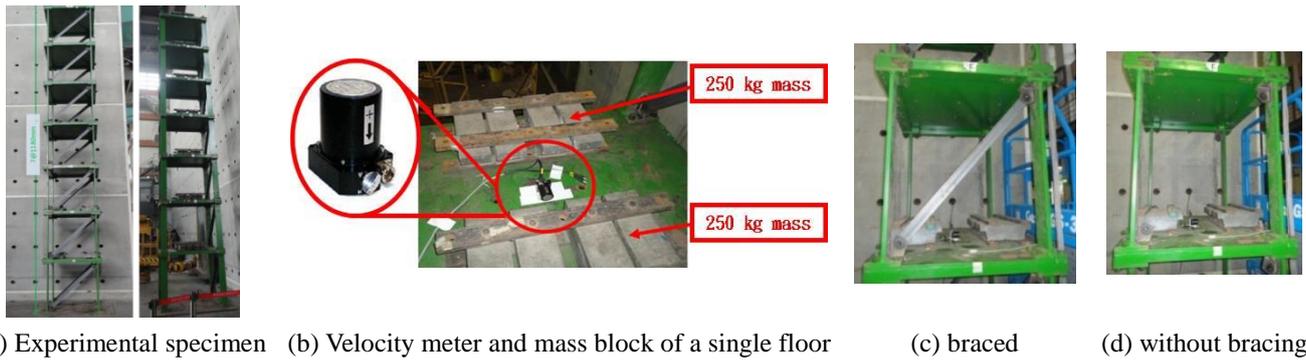
(a) Experimental specimen   (b) Velocity meter and mass block of a single floor   (c) braced   (d) without bracing

Fig. 2 Layouts of experimental structure

(a) Healthy condition
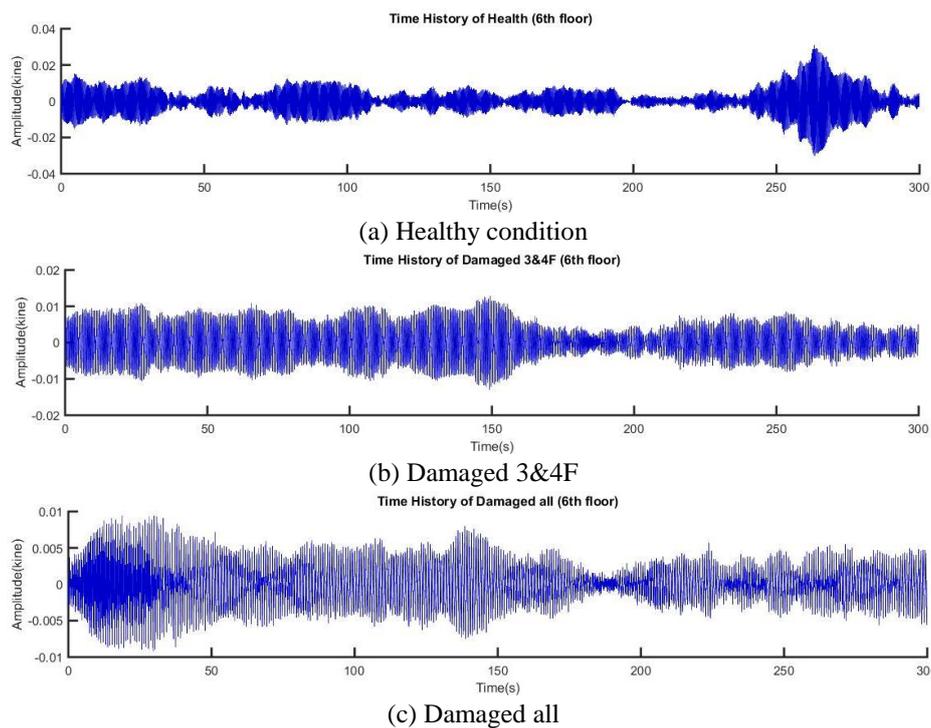
(b) Damaged 3&4F

(c) Damaged all

Fig. 3 Ambient vibration of the 6th floor under different damage cases

possible noise during the test, the environment vibration is conducted during midnight. The data were recorded at a sampling rate of 200 Hz in the longitudinal direction. For each damage case, the total signal recording time was 20 min, which was divided into four segments with each segment being treated as a single run of a specific damage condition. Details of damage in all 6 categories and 16 cases are listed in Table 2. The ambient vibration signal measured from the 6th floor under different damage cases is shown in the Fig. 3. As depicted, no significant variation was observed between different damage cases, which demonstrates the necessity of the proposed SHM system.

4. Evaluation of the proposed SHM system

4.1 Damage condition (MFDFA)

The Hurst exponent derived through the MFDFA procedure was first used to detect the damage condition of

the structure. The minimum and maximum scales were set to two to the power of n, where n varies from 4 to 10, respectively. The range of q-orders value was set from 5 to -5 for the purpose of reflecting the macro and micro fluctuations of the time series. The q-order fluctuation function was then calculated by equation 5. In addition, the Hurst exponents in different q-orders could be estimated by detecting the relationship between the q-order fluctuation and scale. The total Hurst exponents with different q-orders were averaged as an overall exponent for a specific damage case.

The damage conditions evaluated for the 16 damage cases are presented in Figs. 4(a) and (b). Each damage case involved four 5-min segments, which are included in the figure, and the results for each case clearly revealed the existence of damage. The presence of damage can be reflected by an increase in $H(q)$ due the interaction between signals, which shows the long-correlation characteristic.

This trend indicates that the $H(q)$ value of a healthy case is the closest value to 0.5, which represents the absence of a

Table 2 Total damage cases and category

Damage case	Damage Category	Damage Floors	Frequency(Hz)
1	Undamaged	None	3.345
2		1F	2.075
3		2F	2.124
4		3F	2.124
5	Slight damage	4F	2.295
6		5F	2.612
7		6F	2.881
8		7F	3.198
9		1 & 2F	1.636
10	Moderate-damage	3 & 4F	1.831
11		5 & 6F	2.319
12		1 & 2 & 3F	1.44
13	Severe-damage	4 & 5 & 6F	1.88
14	Ultimate	1 & 2 & 3 & 4F	1.33
15	damage	4 & 5 & 6 & 7 F	1.855
16	All damage	1-7F	1.245

(a) The average $H(q)$ from UD to 7F

(b) The average $H(q)$ from 12F to AD

Fig. 4 Distribution of Hurst exponent for different damage cases

long-range correlation; specifically, all floors on the structure have virtually uncorrelated behavior which means the behavior of each floor does not affected by any damage on the structure. If the damage exists, the signal of the undamaged floor will be impacted by the damaged floor that causes the long memory between two signals. The damage on the first floor (1F), which could have a larger contribution to the global structural behavior when compared with the damage on the second floor (2F) was more closely associated with a higher $H(q)$ value. However, in the slightly damaged case, where the damage on the higher floor, fifth, sixth, and seventh floor, the $H(q)$ value is close to the healthy case. As the high-story damage has less contribution to the global structural behavior, this phenomenon may be caused by the varying environmental conditions (temperature, humidity) and the boundary condition between structure and ground, which make the $H(q)$ value fluctuated. It also demonstrates that structures with insignificant damage is still a tough task for the existing SHM methods.

Similar trends could also be observed in other damage conditions. Cases with damage on the first and second floors (12F) demonstrated a significantly higher $H(q)$ value than that of cases with damage on the third and fourth floors (34F) and fifth and sixth floors (56F). Only a minor error was observed for damage on the second floor (2F), which showed a lower value than that of the third floor (3F). Therefore, when $H(q)$ is applied, the possible damage condition can be rapidly detected. The comparison of $H(q)$ value is a relative method to determine the damage condition. The initial measured data, referred as a health structure, is critical to the quantification of different levels of damage.

4.2 Damage location (MFDXA)

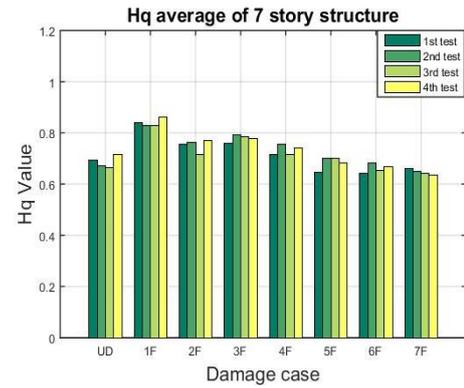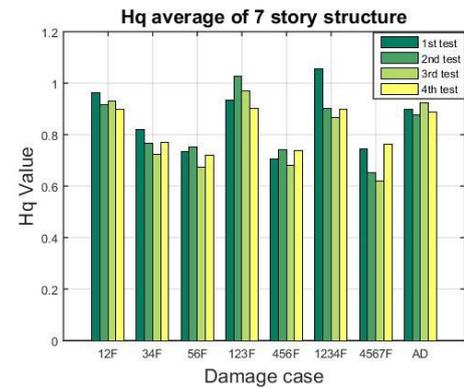MFDXA was employed to identify the damage location. From the seven-story structure, eight MFDXA curved surfaces, namely $G*G$, $G*1F$, $G*2F$, $G*3F$, $G*4F$, $G*5F$, $G*6F$, and $G*7F$, were generated through a cross-correlation procedure between the ground signal and other signals. The healthy structure was first analyzed. The increment between adjacent surfaces, calculated by subtracting the curved surface for a particular floor (e.g., $G*G$) from the curved surface for the floor above (e.g., $G*1F$), was recognized as a reference in the MFDFA method, as shown in Fig. 5(a). This figure implies that the increment of covariance on each floor did not indicate significant differences between surfaces under the healthy condition.

The damage diagnosis result for the first floor (1F) is shown in Fig. 5(b). The result clearly reveals that the first floor surface increased precipitously, meaning the similarity between the first floor and the other floors sharply declined, whereas the other surfaces remained similar to each other. Compared with the increment of reference, this trend shows the presence of damage on the first floor. Fig. 5(c) presents the case with damage on the third and fourth floors (34F). The jump of surfaces on the third and fourth floors indicated the occurrence of damage on these floors, in addition to implying a decrease in behavioral similarity between the third floor, fourth floor, and other floors.

Similar trends were observed, as illustrated in Fig. 5(d), which represents the case of damage from the first floor to the third floor (123F). The surfaces of increment for the first, second, and third floors ascended rapidly, which formed a wide region between these and the other floors.
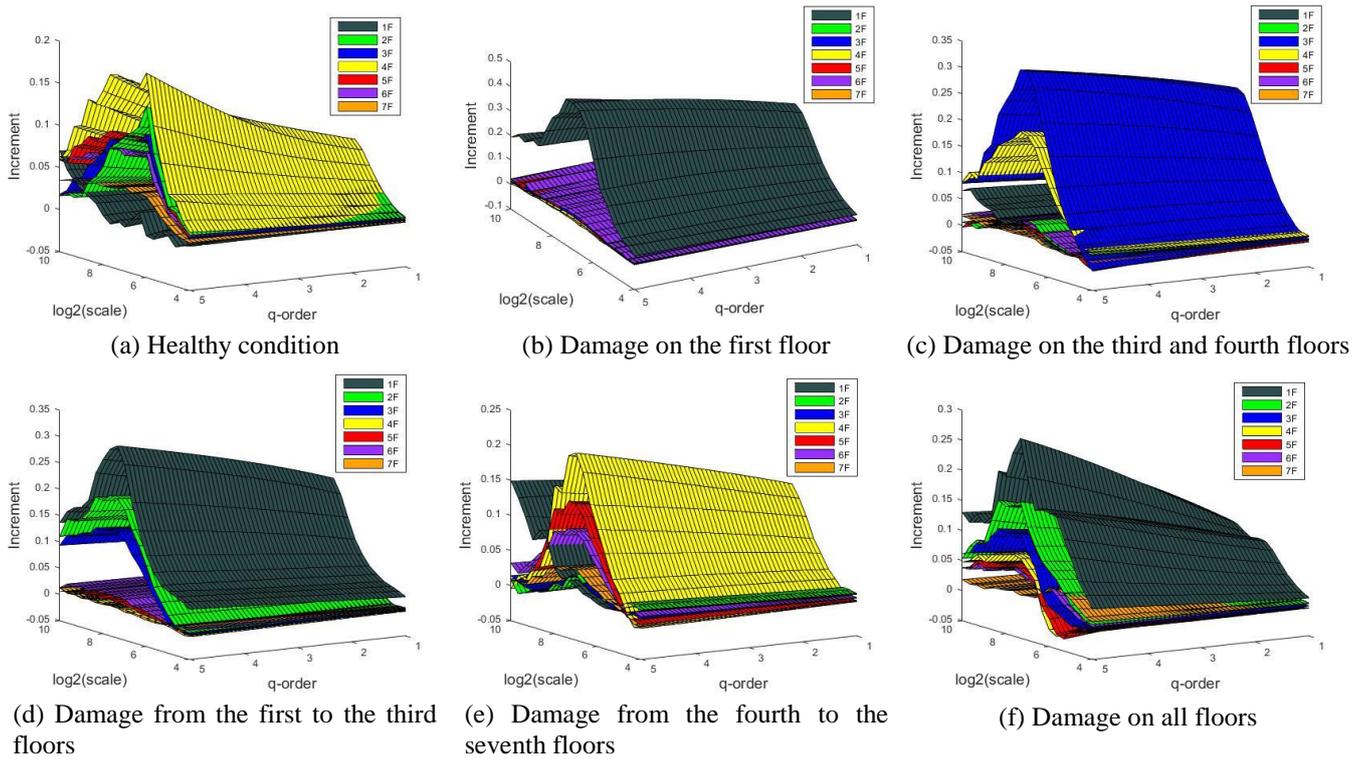
(a) Healthy condition

(b) Damage on the first floor

(c) Damage on the third and fourth floors

(d) Damage from the first to the third floors

(e) Damage from the fourth to the seventh floors

(f) Damage on all floors

Fig. 5 Experimental MFDXA curved surfaces

Table 3 The accuracy of MFDXA and damage index method for different noise levels

Damage location	SNR=60		SNR=40		SNR=20	
	MFDXA	Damage index	MFDXA	Damage index	MFDXA	Damage index
1F	C	C	C	C	C	C
2F	C	C	C	C	C	C
3F	C	C	C	C	C	C
4F	C	C	C	C	C	C
5F	C	C	C	C	C	C
6F	C	C	C	C	C	C
7F	F	C	F	C	F	C
1&2F	C	C	C	C	C	C
3&4F	C	C	C	C	C	C
5&6F	C	C	C	C	C	C
1&2&3F	C	C	C	C	F	C
4&5&6F	C	C	C	C	F	F
1&2&3&4F	C	C	C	C	C	C
4&5&6&7F	F	C	F	C	F	F
Damaged all	F	F	F	F	F	F
Accuracy(%)	80%	93.33%	80%	93.33%	66.67%	73.33%

Moreover, a phenomenon was noticed that the increment of the low-floor damage is larger than that of the high-floor damage in the Fig. 5(c) and (d). It could be resulted from the significant contribution of the low-floor damage to the whole structure. However, the results of the cases of damage from the fourth floor to the seventh floor did not follow the expected trend; an error was observed on the surface of the seventh floor, which did not form a region between the other undamaged floors, as shown in Fig. 5(e). As the damage on the top floor only has a slight impact on the structure, which may be obscured as the environmental interferences, misjudgment was perceived. Furthermore, in all damage cases, the seven surfaces did not follow this trend; the increment between adjacent surfaces did not present an obvious damage as in other cases.

4.3 Damage location (Damage index)

Although most of the damage locations could be distinguished by the MFDXA surfaces, the absence of quantization renders this method unpersuasive. Therefore, the proposed damage index was employed to improve the reliability and practicability of the SHM system. The damage index values for the five selected cases are provided in Fig. 6.

As shown in Fig. 6(a), negative damage index values clearly occurred on the first floor, while the other index values remained positive. This phenomenon was caused by the stiffness reduction, which was set by removing the brace on the first floor. Hence, the change on the first floor was different from that observed under the healthy condition. The damage location could be detected by the damage index.

Similar trends were observed in the case of damage on the third and fourth floors, where the proposed damage index accurately detected damage locations (Fig. 6(b)). Negative values were observed on the third and fourth floors while the other floors remained positive. As expected, the case of damage from the first floor to the third floor was also diagnosed correctly (Fig. 6(c)). The damage index
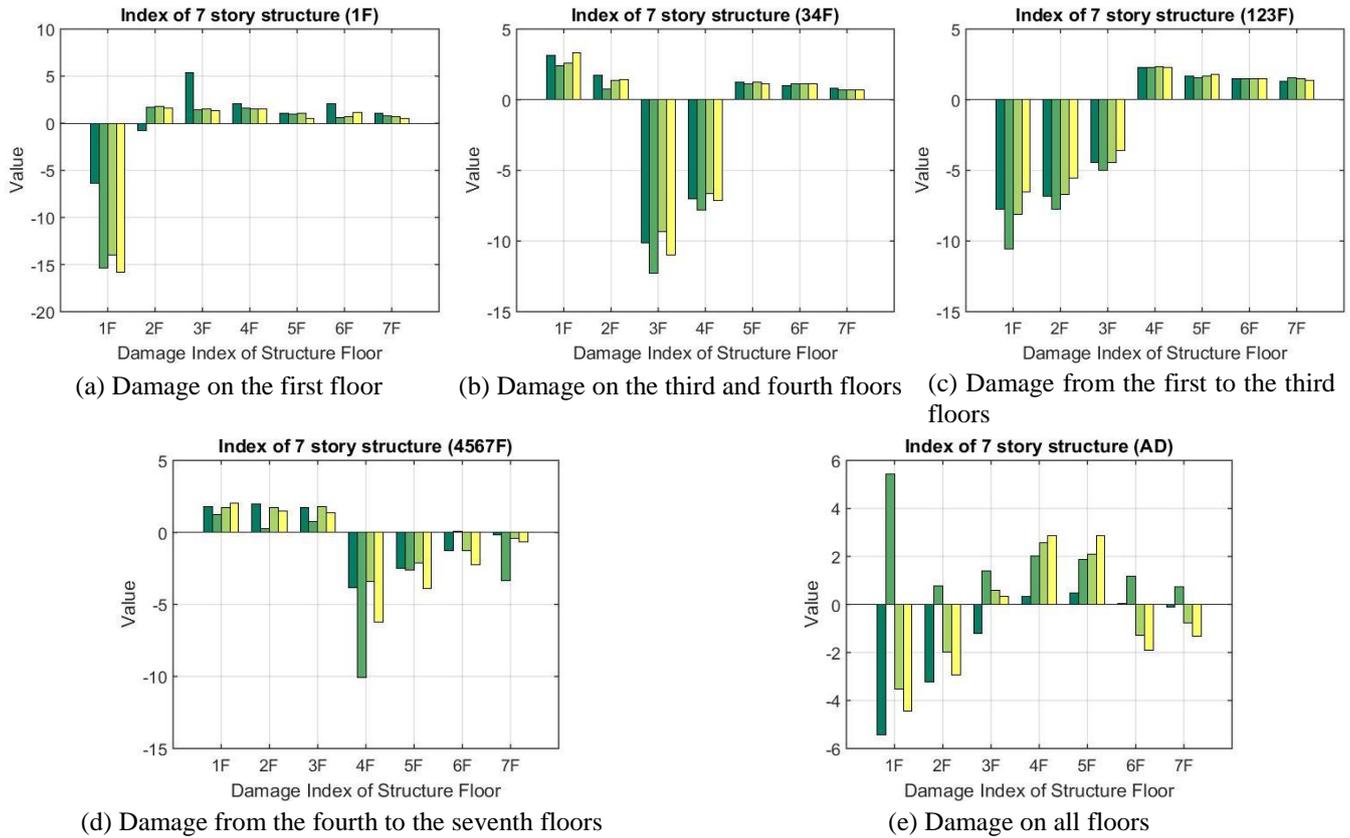
(a) Damage on the first floor

(b) Damage on the third and fourth floors

(c) Damage from the first to the third floors

(d) Damage from the fourth to the seventh floors

(e) Damage on all floors

Fig. 6 Damage index of experimental conditions

Table 4 Damage location detection for different methods

Damage Location	Method			
	Detrended Cross-Correlation Analysis (DCCA)	Damage Index (DCCA)	Multifractal Detrended Cross-Correlation Analysis (MFDXA)	Damage Index (MFDXA)
1F	C	C	C	C
2F	C	C	C	C
3F	C	C	C	C
4F	C	C	C	C
5F	C	C	C	C
6F	F(2&6F)	F(5&6F)	C	C
7F	F(1&2&3F)	C	F(7F)	C
1&2F	C	C	C	C
3&4F	C	C	C	C
5&6F	C	C	C	C
1&2&3F	C	C	C	C
4&5&6F	C	C	C	C
1&2&3&4F	C	C	C	C
4&5&6&7F	F(4&5&6F)	C	F(7F)	C
Damaged all	F(1&2&3&4F)	F(2&3&4&7F)	F(all floors)	F(3&4&5&6F)
Accuracy(%)	75%	87.5%	80%	93.33%

* C: Correct,
  F: False

values of the damaged floors were negative, whereas those of the undamaged floors were positive.

Fig. 6(d) shows the damage index for damage from the fourth floor to the seventh floor. Most of the damaged floors could be detected; only the signal recorded in the second 5-min segment had an extremely low positive value on the sixth floor, and therefore caused misjudgment; however, as shown in the Fig 6(e), misjudgment occurred for damage on all floors The damage index revealed complex manners compared with the preceding damage cases. The all damaged case could be considered as another type of healthy case with insignificant correlation between each floor, indicating that the stiffness of each floor was approximately equivalent.

Furthermore, to ensure the practical robustness of the proposed MFDXA method, different levels of noise are randomly added into the original time series to evaluate the effect of noise interference. The noise is generated by utilizing a Gaussian white-noise; the signal-to-noise ratio (SNR) values are chosen to be 60 dB, 40dB, and 20dB. The evaluation is performed by examining whether the damage location can be correctly diagnosed by the MFDXA and damage index methods. As shown in the Table 3, the accuracy of the method based on MFDXA remains a great performance under the cases of SNR 60 and 40; however, the accuracy decreases to 66.67% under SNR20. The performance of the damage index supports the same result under SNR 60 and 40. For a higher noise level (SNR 20), the damage index provides a robust result on damage location assessment compared with the MDFXA method.

The result has demonstrated that the proposed methods are reliable under the influence of the possible external noise.

The MFDXA method was compared with other methods of SHM. A total of 15 damage cases were analyzed using the detrended cross-correlation analysis (DCCA) method, DCCA-based damage index, MFDXA, and the proposed damage index, and the results are listed in Table 4 (Fajri and Lin 2015). As indicated, the accuracy rates of DCCA and the DCCA-based damage index were 75% and 87.5%, respectively; nevertheless, the accuracy rate of MDFXA was 80%. In addition, the proposed damage index could improve the accuracy to 93.33%, and only the case of all floors being damaged failed, the result showed that by utilizing multifractality, a SHM method more reliable than the DCCA method is provided.

5. Conclusions

By adopting multifractal analysis, which can interpret complex, irregular, and disordered phenomena, a SHM system based on MFDFA and MFDXA is proposed. MFDFA was employed to determine the damage condition of a structure, and the Hurst exponent value, an important parameter in MFDFA, was applied to show the degree of damage. MFDXA was also used to localize the damage location in the structure. The detrended covariance, derived from the MFDXA algorithm, was utilized to identify the damage location. Additionally, the proposed damage index could quantify the damage location and simplify the diagnosis process.

An experimental verification was carried out on a seven-story scaled-down benchmark structure at NCREE. Sixteen damage cases were executed and analyzed. On the basis of the MFDFA method, the damage condition could be assessed through H(q). Moreover, the damage location could be localized using the MFDXA technique with 80% accuracy, and the accuracy could be further improved to 93.33% when the proposed damage index was employed. As only ambient vibration signal is required as a set of initial reference measurements, the proposed system offers an easy and alternative strategy for practical SHM.

References

Aktan, A. and Catbas, F. (2003), "Development of a model health monitoring guide for major bridges", Fed. High. Adm. Res. Dev., no. DTFH61-01-P-00347. July, 1-290.

Dutta, S., Ghosh, D. and Chatterjee, S. (2013). "Multifractal detrended fluctuation analysis of human gait diseases", *Front. Phys.*,**4**,1-7.

Dutta, S., Ghosh, D. and Samanta, S. (2016), "Non linear approach to study the dynamics of neurodegenerative diseases by Multifractal Detrended Cross-correlation Analysis- A quantitative assessment on gait disease", *Physica A*, **488**, 181-195.

Fajri, H. and Lin, T.K. (2017), "Damage detection of sStructures with detrended fluctuation and detrended cross-correlation analyses", *Smart Mater. Struct.*, **26**(3), 1-19.

Fan, W. and Qiao, P. (2011), "Vibration-based damage identification methods : A review and comparative study",

10(1), 83-111.

Farrar, C.R. and James, G.H. (1997), "System identification from ambient vibration measurements on a bridge", *J. Sound Vib.*, **205**(1), 1-18.

Ghosh, D., Dutta, S. and Chakraborty, S. (2014), "Multifractal detrended cross-correlation analysis for epileptic patient inseizure and seizure free status", *Chaos Solit. Fracat.*, **67**, 1-10.

Haris, K., Chakraborty, B., Menezes, A., Sreepada, R.A. and Fernandes, W.A. (2014), "Multifractal detrended fluctuation analysis to characterize phase coupling in seahorses (Hippocampus kuda) feeding clicks", *Acoust. Soc. Am.*, **136**, 1972-1981.

He, L.Y. and Chen, S.P. (2011), "Multifractal detrended cross-correlation analysis of agricultural future markets", *Chaos Solit. Fracat.*, **44**, 355-361.

Ihlen, E.A.F. (2012). "Introduction to multifractal detrended fluctuation analysis in Matlab", *Front. Phys.*, **3**, 1-18.

Ivanov, P.Ch., Nunes Amaral, L.A., Goldberger, A.L., Havlin, S., Rosenblum, M.G., Struzik, Z.R. and Eugene Stanley, H. (1999), "Multifractality in human heartbeat dynamics", *Macmillan Magazines*, Ltd, **399**, 461-465.

Jang, S.A., Sim, S. and Spencer Jr, B.F. (2007), *Structural Damage Detection Using Static Strain Data*.

Kantelhardt, J.W. (2008), "Fractal and multifractal time series", *Encyclopedia of Complexity and Systems Science*, Springer New York.

Kantelhardt, J.W., Zschiegner, S.A., Koscielny-Bunde, E., Havlin, S., Bunde, A. and Stanley, H.E. (2002), "Multifractal detrended fluctuation analysis of nonstationary time series", *Physica A*, **316**, 87-144.

Li, J., Hao, H., Xia, Y. and Zhu, H.P. (2015), "Damage assessment of shear connectors with vibration measurements and power spectral density transmissibility", *Struct. Eng. Mech.*, **54**(2), 257-289.

Mandelbrot, B.B. (1983), "The fractal geometry of nature", *Am. J. Phys.*, **51**(3), 286-287.

Nie, Q., Xu, J.H. and Man, W. (2016), "Long-range cross-correlation between urban impervious surfaces and land surface tempertures", *Front. Earth. Sci.*, **10**(1), 117-125.

Pandey, A.K., Biswas, M. and Samman, M.M. (1991), "Damage detection from changes in curvature mode shapes", *J. Sound Vib.*, **145**(2), 321-332.

Pehlivan, H. and Bayata, H.F. (2016), "Usability of inclinometers as a complementary measurement tool in structural monitoring", *Struct. Eng. Mech.*, **58**(6), 1077-1085.

Peng, C.K., Buldyrev, S.V., Goldberger, A.L., Havlin, S., Mantegna, R.N., Simons, M. and Stanley, H.E. (1995), "Statistical properties of DNA sequences", *Physica A*, **221**, 180-192.

Peng, C.K., Havlin, S., Stanley, H.E. and Goldberger, A.L. (1995), "Quantification of scaling exponents and crossover phenomena in nonstationary heartbeat time series", *Am. Inst. Phys.*, **5**(1), 82-87.

Sadegh Movahed, M. and Hermanis, E. (2008), "Fractal analysis of river flow fluctuations", *Physica A*, **387**, 915-932.

Shadkhoo, S. and Jafari, G.R. (2009), "Multifractal detrended cross-correlation analysis of temporal and spatial seismic data", *Eur. Phys. J. B*, **72**, 679-683.

Su, H.Z., Wen, Z.P., Wang, F. and Hu, J. (2016), "Dam structural behavior identification and prediction by using variable dimension fractal model and iterated function system", *Appl. Soft Comput.*, **48**, 612-620.

Wang, F., Liao, G.P. and Zhou, X.Y. (2013), "Multifractal detrended cross-correlation analysis for power markets", *Nonlin. Dyn.*, **72**(1), 353-363.

Yan, A.M., Kerschen, G., Boe, D. and Golinval, J.C. (2005),

"Structural damage diagnosis under varying environmental conditions-Part I: A linear analysis", *Mech. Syst. Signal Pr.*, **19**(4), 847-864.

Yun, G.J. (2012), "Detection and quantification of structural damage under ambient vibration environment", *Struct. Eng. Mech.*, **42**(3), 425-448.

Zhou, W.Z. (2008), "Multifractal detrended cross-correlation analysis for two nonstationary signals", *Phys. Rev.*, E**77**, 066211.